ELSEVIER

Turbulent heat transfer in a square duct

M. Hirota and H. Fujita
Department of Mechanical Engineering, Nagoya University, Chikusa-ku, Nagoya, Japan

H. Yokosawa
School of Informatics and Sciences, Nagoya University, Chikusa-ku, Nagoya, Japan

H. Nakai
Chubu Electric Power Co. Ltd., Higashi-ku, Nagoya, Japan

H. Itoh
Nippon Steel Corp., Chiyoda-ku, Tokyo, Japan

The characteristics of the flow and temperature fields in turbulent flow through a straight duct with a square cross section are considerably complex owing to the momentum and heat transport by the secondary flow of the second kind. For a basic understanding of the turbulent heat transport process in such a complex turbulent flow, the detailed characteristics of the turbulent temperature field must be made clear. This paper presents experimental results concerning the fluctuating temperature intensity, cross-correlation coefficients between the fluctuating velocity and temperature, and the turbulent heat fluxes obtained for forced-convection heat transfer in a square duct. The contours of the turbulent heat flux in the streamwise direction are distorted greatly toward the duct corner, similar to those of the fluctuating temperature intensity. Similarity has been also found between the distributions of the turbulent heat flux in the transverse direction and the turbulent shear stress. Based on the results of the measurements, the eddy-viscosity, eddy thermal diffusivity, and turbulent Prandtl number have been also obtained. The distributions of the eddy-diffusivities and turbulent Prandtl numbers on the symmetric axis of a square duct are similar to those in a circular pipe. As the duct corner is approached, however, the eddy-diffusivities become smaller, and the turbulent Prandtl number becomes larger, and thus the assumption of the constant turbulent Prandtl number is invalid for turbulent heat transfer in a square duct.

Keywords: turbulent heat transfer; square duct; secondary flow; turbulent heat flux; eddy thermal diffusivity; turbulent Prandtl number

Introduction

In turbulent flow through a straight duct with a noncircular cross section, secondary flow of Prandtl's second kind is caused by the anisotropy of the turbulent stresses (Johnston 1976). Although this secondary flow is very weak, at most a few percent of the primary flow velocity, it exerts a great influence on the flow field in the duct. Many experimental and numerical studies have been conducted on turbulent flow through a square duct, which is a noncircular duct with a relatively simple cross-sectional geometry, to make clear the flow characteristics accompanied by secondary flow of the second kind (Launder and Ying 1973; Gessner and Emery 1976; Gessner and Po 1976; Gessner et al. 1979; Melling and Whitelaw 1976; Gessner 1981; Nakayama et al. 1983; Demuren and Rodi 1984; Speziale 1987; Nishijima 1989; Hayase and Suematsu 1991; Kajishima et al. 1991; Madabhushi and Vanka 1991; Myong 1991; Gavrilakis 1992; Huser and Biringen 1993; Sugiyama et al. 1993; Huser et al. 1994.) These studies have made clear the detailed characteristics of turbulent flow in the duct and have revealed that the turbulent stress field becomes considerably complex owing to the occurrence of the secondary flow.

In forced-convection heat transfer for turbulent flow in a square duct, the thermal energy is also transported by secondary flow of the second kind. Therefore, it is expected that the characteristics of the temperature field as well as the flow field become more complex than those in a circular pipe and a two-dimensional (2-D) channel. However, very few data have been presented on the temperature field for turbulent heat transfer in a square duct. Brundrett and Burroughs (1967) first made clear experimentally the distributions of the mean temperature in a square duct and revealed that the influences of the

Address reprint requests to Prof. M. Hirota, Department of Mechanical Engineering, Nagoya University, Chikusa-ku, Nagoya 464-01, Japan.

Received 10 March 1996; accepted 17 October 1996

Int. J. Heat and Fluid Flow 18:170–180, 1997

655 Avenue of the Americas, New York, NY 10010

0142-727X/97/$17.00
PII S0142-727X(96)00151-8

secondary flow appear in the local wall heat-flux distributions. In numerical simulations, Launder and Ying (1973), Nakayama and Koyama (1986), and Myong (1991) calculated the mean temperature distributions in the duct assuming that the turbulent Prandtl number is constant over the duct cross section. Emery et al. (1980) also calculated the mean temperature distribution in a square duct and compared their numerical results with experiment (Alexopoulos 1964). Fujita et al. (1988) made the numerical simulation for turbulent flow and heat transfer in a square duct with two roughened facing walls. Sugiyama et al. (1995) also performed a numerical analysis for the square duct with one rough wall using a turbulent heat-flux model and predicted distributions of the turbulent heat fluxes in the duct. The authors conducted an experimental study on turbulent flow and heat transfer in a square duct with a rough wall and have made clear the influences of the secondary flow on the mean temperature field (Fujita et al. 1989; Yokosawa et al. 1989; Fujita et al. 1990; Hirota et al. 1994).

In general, turbulent heat transfer in the duct is dominated by the transport of heat by turbulence. Therefore, in order to understand the mechanism of turbulent heat transfer in the complex flow through a square duct, the characteristics of the turbulent temperature field, such as temperature fluctuation intensity and turbulent heat fluxes, should be examined in detail. To the authors' knowledge, however, there have been no experimental data on the turbulent temperature field for turbulent heat transfer in a square duct. With these points as background, we have made attempts to make clear experimentally the characteristics of turbulent temperature field for forced-convection heat transfer in a straight duct with a square cross section. In this paper, we show the measured results of temperature fluctuation intensity, cross-correlation coefficients between fluctuating velocity and temperature, and turbulent heat fluxes. Based on these data, the characteristics of the eddy-diffusivities and turbulent Prandtl numbers are also discussed. The data presented in this paper are important not only for the basic understanding of the turbulent heat transport process in a square duct, but also for testing and improving turbulent heat transfer models used to simulate the heat transfer in complex turbulent flows.

Experiments

Figure 1 is a schematic diagram of the experimental apparatus. The flow system is almost the same as that used in preceding experiments (Hirota et al. 1994). Air at room temperature flows into the straight test duct through a quadrant nozzle flow meter

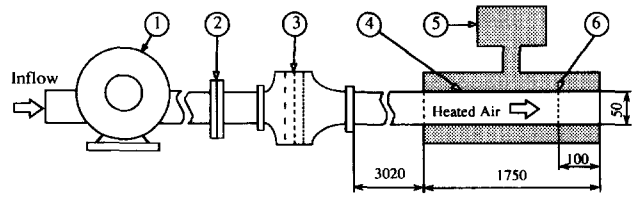

Figure 1 Schematic diagram of the experimental apparatus; (1) turbo fan; (2) quadrant nozzle flow meter; (3) settling chamber; (4) test duct (heated part); (5) steam boiler; (6) measuring cross section

and a settling chamber. The test duct has a square cross section of 50×50 mm and a length of 4770 mm = 95.4 D. The walls of the test duct are hydraulically smooth. The test duct includes a heated part between the duct exit and 1750 mm ($= 35\ D$) upstream from the exit. The heated part has a double concentric duct structure and the inner duct is the test duct in which the velocity and temperature fields are measured. All walls of the inner duct, which are made of 10 mm-thick smooth aluminum plates, are heated isothermally at a temperature of 373 K by the condensation of saturated steam supplied between the inner and outer (jacket) ducts. To confirm that the isothermal heating condition is satisfied with high accuracy, wall temperature distributions were measured over the heated part with 52 thermocouples. The scattering of the measured wall temperature was less than 0.3°C, and, thus, the condition of isothermal heating was satisfied almost exactly.

Figure 2 shows the coordinate system. The mean velocities in each direction are denoted as U_1, U_2, and U_3 and the fluctuating velocities as u_1, u_2, and u_3. The measuring cross section is a quadrant of the flow located 100-mm upstream from the duct exit, in which the flow and temperature fields are both fully developed. We have conducted the experiments at a Reynolds number $\mathrm{Re} = U_b \cdot D/\nu$ of 6.5×10^4, where U_b and ν denote the bulk velocity and kinetic viscosity of air, respectively, defined at the entrance of the heated part. The fluctuating velocities and fluctuating temperature were measured simultaneously by multiple-wire probes which consist of the I-type or X-type hot wires (anemometer) and the I-type cold wire (thermometer). The output signals from those wires were separated into the instantaneous velocities and temperature by digital processing based on the scheme developed by Hishida and Nagano (1978). The active lengths of the hot wire and cold wire are 0.8 and 1.7 mm, respectively. Two types of X-wire anemometer probes were used

Notation

B	$D/2$ (= 25 mm)
D	side length of duct cross section = hydraulic diameter of the duct
Pr_{t2}	turbulent Prandtl number, Equation 6
R_{1t}	correlation coefficient between u_1 and t, Equation 3
R_{2t}	correlation coefficient between u_2 and t
R_{3t}	correlation coefficient between u_3 and t
R_{12}	correlation coefficient between u_1 and u_2
T	time-mean temperature of fluid
T_C	time-mean temperature of fluid at the duct center
T_W	wall temperature
T^+	dimensionless time-mean temperature of fluid $=(T_W - T)/T^*$ (T^*: friction temperature)
t	fluctuating temperature of fluid
U_1, U_2, U_3	time-mean velocity component in the X_1-, X_2-, and X_3-directions
U^+	dimensionless time-mean velocity $= U_1/U^*$ (U^*: friction velocity)
u_1, u_2, u_3	fluctuating velocity component in the X_1-, X_2-, and X_3-directions
X_1, X_2, X_3	coordinate system, Figure 2
Y^+	dimensionless wall distance $= U^* \cdot Y/\nu$ (Y: wall distance)

Greek

ε_{H2}	eddy thermal diffusivity, Equation 5
ε_{M2}	eddy-viscosity, Equation 4

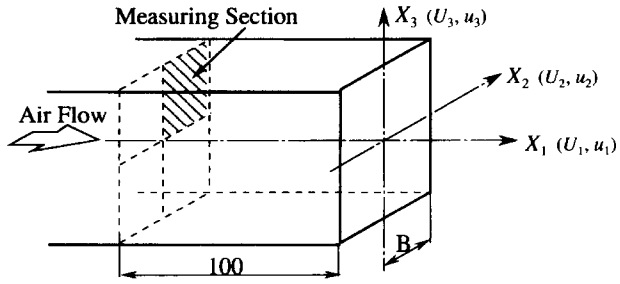

Figure 2 Coordinate system; the shaded area shows the measuring section

to eliminate the experimental errors caused by velocity gradients (Hirota et al. 1988). Figure 3 shows a comparison of the mean and fluctuating velocities measured outward from the wall under isothermal (unheated) and heated conditions along the traverse $X_2/B = 0.8$. The distributions of the measured velocities agree well with each other irrespective of the thermal conditions. This proves that the separation scheme of the velocity and temperature signals used in the present experiment works well and also that the variations of the fluid properties caused by the heating do not exert serious influences on the flow field in the test duct. The probe was traversed along the lines which were parallel to the X_2- or X_3-axis. The interval between the traversing lines was 5 mm, and thus there were ten traversing lines in a quadrant of the duct cross section; that is, X_2 (X_3)$/B = 0$, 0.2, 0.4, 0.6, and 0.8. The number of measurement points set on each traversing line was 22 for X-type hot-wire probe and 27 for I-type hot-wire probe, and, therefore, the contour maps were plotted based on 220 or 270 experimental data in a quadrant. The traversing pitch of the probe became smaller as the wall was approached, and the minimum pitch was 0.25 mm.

Because the results of measurement were symmetric with respect to the X_2- and X_3-axes; i.e., axes of symmetry of the duct, we show the results obtained in a quadrant cross section of the test duct ($X_2 > 0$ and $X_3 > 0$, shaded area in Figure 2). The coordinates in the transverse direction are reduced to be dimensionless by the half of the side length $B = D/2 = 25$ mm.

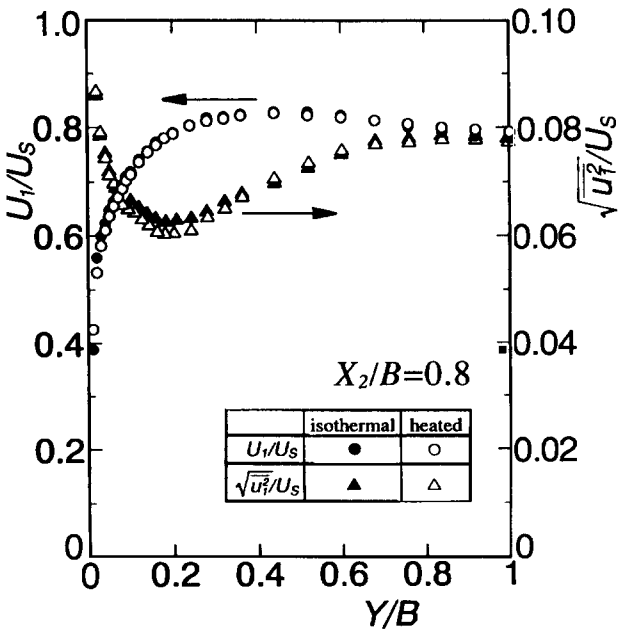

Figure 3 Comparison of the mean and fluctuating velocities measured in isothermal (unheated) and heated flows

Results and discussion

Mean velocity and temperature distributions

Figure 4 shows a contour map of the time-mean primary flow velocity U_1/U_C measured in the heated flow condition. As is well known, due to the effects of momentum transport by secondary flow of the second kind, the U_1 contours are curved outward from the wall on the X_2- and X_3-axes and bulge toward the duct corner on the diagonal (e.g., Melling and Whitelaw 1976). The characteristics of the present U_1-contours measured in the heated flow condition agree well with those of the isothermal flow, which indicates that buoyancy influences are negligibly small for the present experimental condition.

Figure 5 is the contour map of the time-mean temperature $(T_W - T)/(T_W - T_C)$. The mean temperature distribution is quite similar to that of the primary flow velocity. If we compare them in detail, however, it is found that the distortion of the temperature contours is somewhat smaller than that of the mean velocity. This suggests that the influences of the secondary flow on heat transport are weaker than those on momentum transport.

Based on the mean velocity and temperature distributions obtained along lines normal to the top wall of the duct; i.e., the lines parallel to the X_3-axis, we have rearranged them into the form of the wall-law with the wall parameters. Figures 6 and 7 show the results for the velocity and temperature distributions, respectively. For the dimensionless mean velocity U^+, similar to the case of isothermal flow, the velocity distribution in the interval $30 < Y^+ < 300$ over a wide range of X_2/B can be expressed by Sarnecki's equation (Patel 1965) shown below.

$$U^+ = 5.5 \log Y^+ + 5.4 \tag{1}$$

A similar result is obtained for the mean temperature, and the T^+-distribution in the interval $30 < Y^+ < 300$ can be represented as follows.

$$T^+ = 4.98 \log Y^+ + 4.48 \tag{2}$$

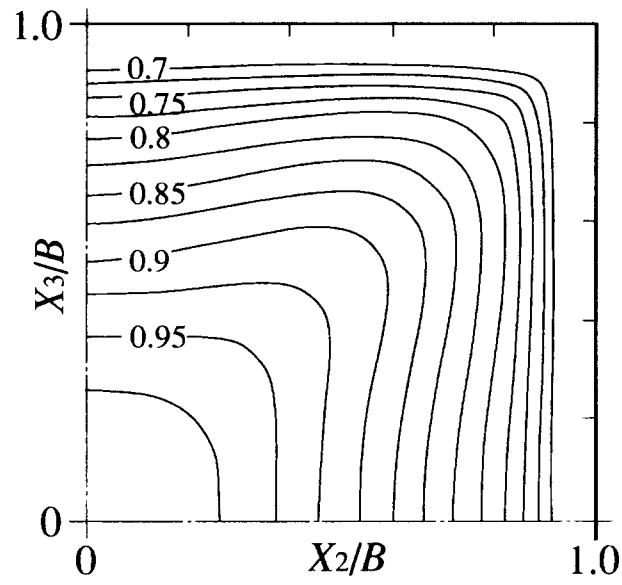

Figure 4 Mean primary flow velocity, U_1/U_C

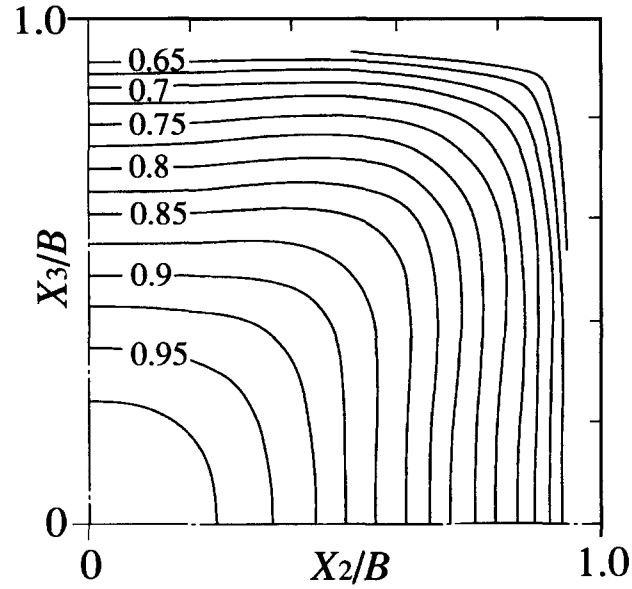

Figure 5 Mean temperature, $(T_W - T)/(T_W - T_C)$

This distribution of T^+ is quite similar to that obtained in turbulent heat transfer through a pipe with a circular cross section (Hishida and Nagano 1979).

Intensities of fluctuating velocity and fluctuating temperature

The rms values of the fluctuating velocity in the X_1-direction u_1, and those of the fluctuating temperature t are shown in Figures 8 and 9, respectively. In both distributions of $\sqrt{\overline{u_1^2}}$ and $\sqrt{\overline{t^2}}$, the contours protrude sharply toward the duct corner, and the distortions of the contours are much stronger than those of U_1 and T. The distribution of $\sqrt{\overline{t^2}}$ is qualitatively similar to that of $\sqrt{\overline{u_1^2}}$, but the values of $\sqrt{\overline{t^2}}/(T_W - T_C)$ are smaller than those of

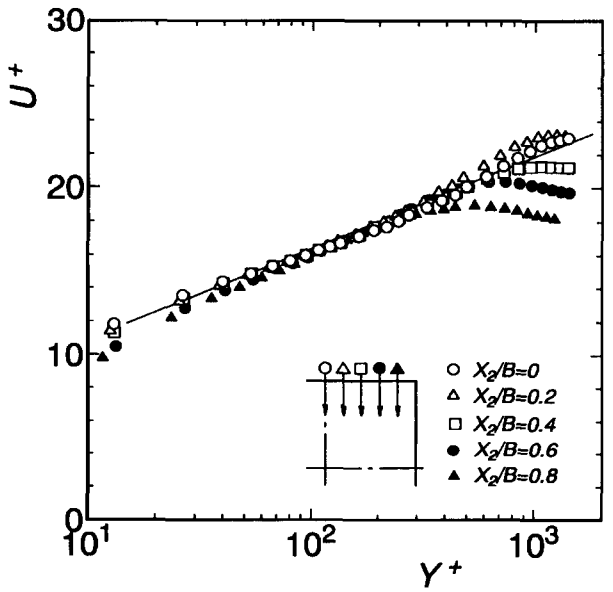

Figure 6 Mean primary flow velocity distributions in wall parameters; (solid line: Sarnecki's equation)

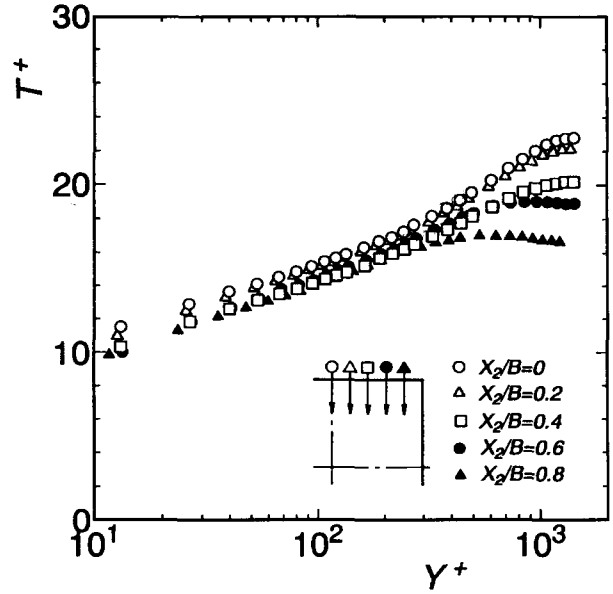

Figure 7 Mean temperature distributions in wall parameters

$\sqrt{\overline{u_1^2}}/U_C$ at the corresponding points in the flow. It has been found that, at the center of the duct, the value of $\sqrt{\overline{t^2}}/(T_W - T_C)$ agrees well with that of $\sqrt{\overline{u_1^2}}/U_C$, and that the values of $\sqrt{\overline{t^2}}/(T_W - T_C)$ near the duct walls are almost the same as those of $\sqrt{\overline{u_2^2}}/U_C$ or $\sqrt{\overline{u_3^2}}/U_C$.

Cross-correlation coefficients between fluctuating velocity and temperature

Figure 10 shows distributions of the cross-correlation coefficient between the fluctuating velocity in the primary flow direction u_1 and the fluctuating temperature t. The abscissa is the dimensionless wall distance Y^+. This cross-correlation coefficient is de-

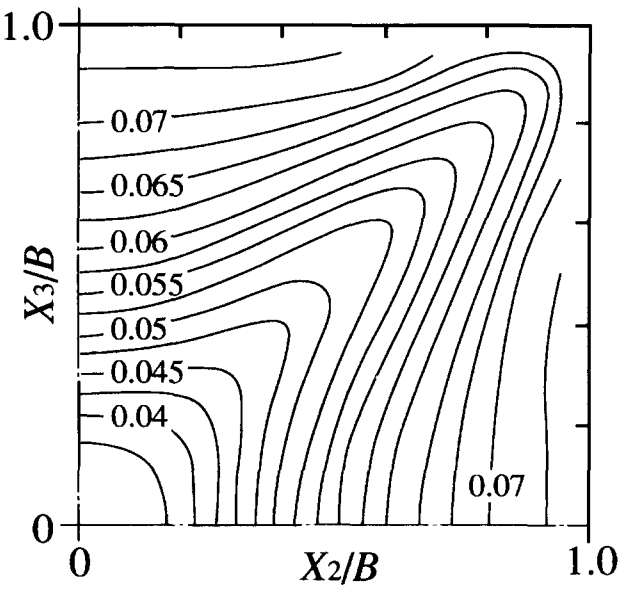

Figure 8 Intensity of fluctuating velocity, $\sqrt{\overline{u_1^2}}/U_C$

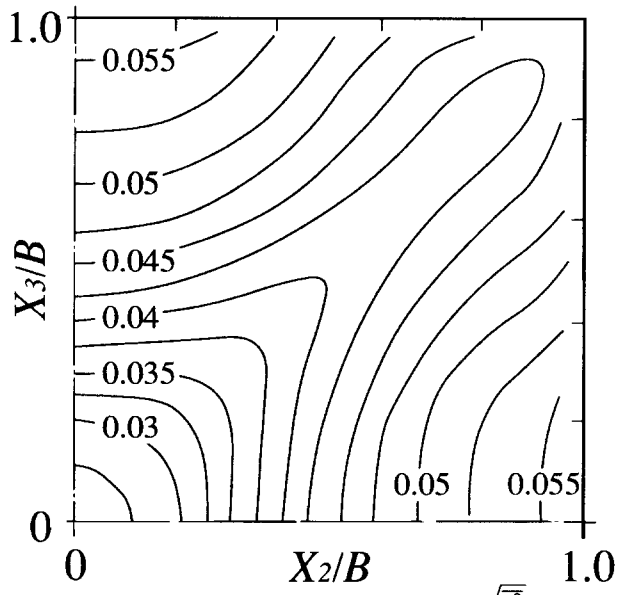

Figure 9 Intensity of fluctuating temperature, $\sqrt{t^2}/(T_W - T_C)$

noted as R_{1t} and defined as follows.

$$R_{1t} = \frac{-\overline{u_1 t}}{\sqrt{u_1^2} \cdot \sqrt{t^2}} \tag{3}$$

On the X_3-axis ($X_2/B = 0$), R_{1t} shows an almost constant value of 0.64 in the region of $Y^+ < 200$ in which the wall law shown in Equations 1 and 2 are valid for U^+ and T^+, and then it decreases rapidly with an increase of Y^+. This distribution of R_{1t} on the X_3-axis is quite similar to that obtained in a smooth circular pipe by Hishida and Nagano (1979), which is shown by the solid line in the figure. As the side wall is approached; i.e., the values of X_2/B are increased, the upper limit of Y^+ at which R_{1t} keeps constant value becomes smaller. In the distributions near the side wall for $X_2/B > 0.4$, the values of R_{1t} once decrease with an increase of Y^+, then attain a local minimum, and again increase with Y^+. The locations at which R_{1t} shows local minimum values correspond to the diagonal of the duct cross section. It is also found that, at least in the buffer layer for $Y^+ < 30$, R_{1t} does not change in the spanwise (X_2-axis) direction and shows almost the constant value of 0.64. This suggests that the influences of an adjacent wall do not appear obviously in the R_{1t} distributions in the near-wall region.

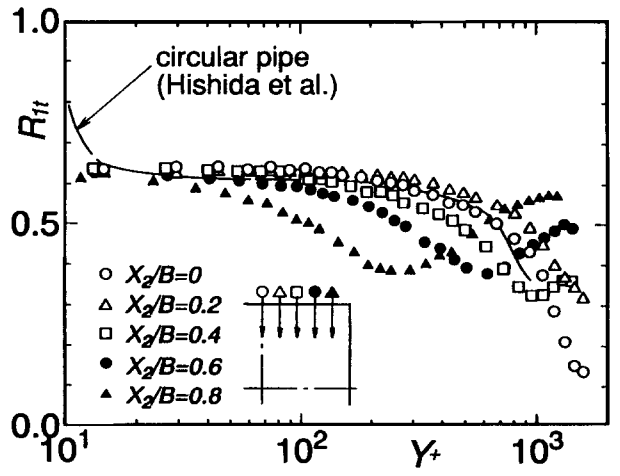

Figure 10 Cross-correlation coefficient between u_1 and t (R_{1t})

Figure 11 shows a contour map of R_{1t}. Similar to the fluctuating intensities $\sqrt{u_1^2}$ and $\sqrt{t^2}$ shown in Figures 8 and 9, the contour lines are greatly distorted toward the duct corner. As estimated from the R_{1t} distribution shown in Figure 10, the values of R_{1t} become smaller with an increase of the distance from the duct walls and attain local minimums on the diagonal of the duct cross section. The region in which R_{1t} shows relatively large values becomes narrower as the duct corner is approached. The regions in which R_{1t} is near the constant value of 0.64 in Figure 10 corresponds to those of $0.85 < X_3/B < 0.99$ on the X_3-axis and of $0.98 < X_3/B < 0.99$ on the line of $X_2/B = 0.8$.

Next, we show the distributions of the correlation coefficients concerning the fluctuating velocity components in the transverse directions. Figure 12 shows $R_{2t} = -\overline{u_2 t}/\sqrt{u_2^2} \cdot \sqrt{t^2}$, the cross-correlation coefficient between u_2 (fluctuating velocity in the horizontal direction) and t. The turbulent heat flux $\overline{u_2 t}$, which appears in the definition of R_{2t}, means the heat transport from the side wall ($X_2/B = 1.0$) by u_2 the turbulent velocity component normal to this wall. Near this side wall, the contour lines of relatively high R_{2t} values are distributed almost parallel to the wall. This means that, near the side wall, which is the main heat transfer surface for $\overline{u_2 t}$, the values of R_{2t} are almost constant in the X_3-direction over a relatively wide range of X_3/B. As the distance from the side wall is increased, the range of X_3/B in which the contour lines lie parallel to the side-wall becomes narrower, and R_{2t} shows smaller values in the region nearer the top wall ($X_3/B = 1.0$). On the other hand, near the intersection of the X_3-axis and the top wall, there appears a region enclosed by the contour of $R_{2t} = 0$, and the sign of R_{2t} in this closed region is reversed with respect to that near the side wall.

Figure 13 shows the distribution of $E_{3t} = -\overline{u_3 t}/\sqrt{u_3^2} \cdot \sqrt{t^2}$, which is related to the turbulent heat transport from the top wall by u_3. The contour lines near the top wall are distributed almost parallel to the wall, and the region enclosed by the lines of $R_{3t} = 0$ exists near the intersection of the X_2-axis and the side wall. It follows that the distributions of R_{2t} and R_{3t} are almost

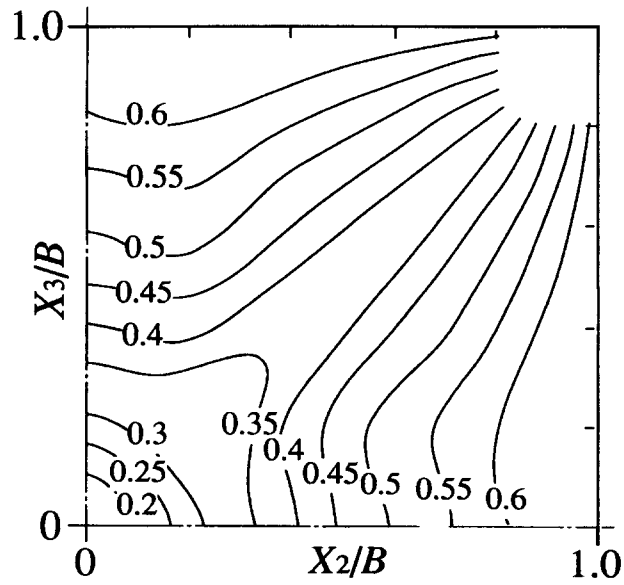

Figure 11 Contour map of R_{1t}

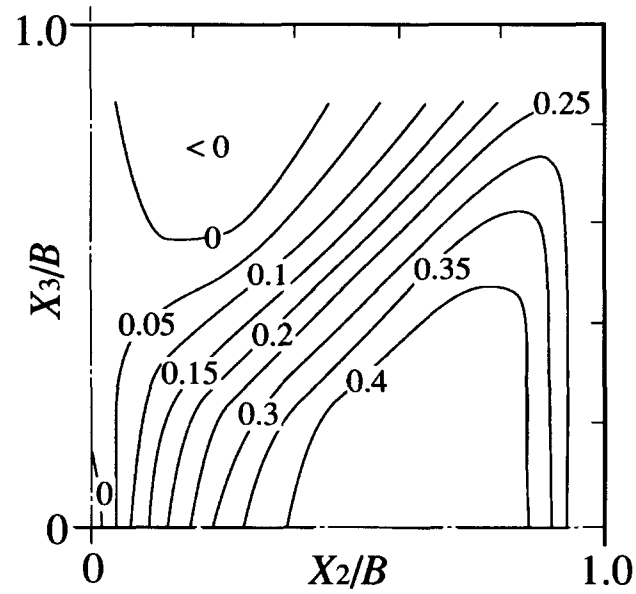

Figure 12 Contour map of R_{2t} (cross-correlation coefficient between u_2 and t)

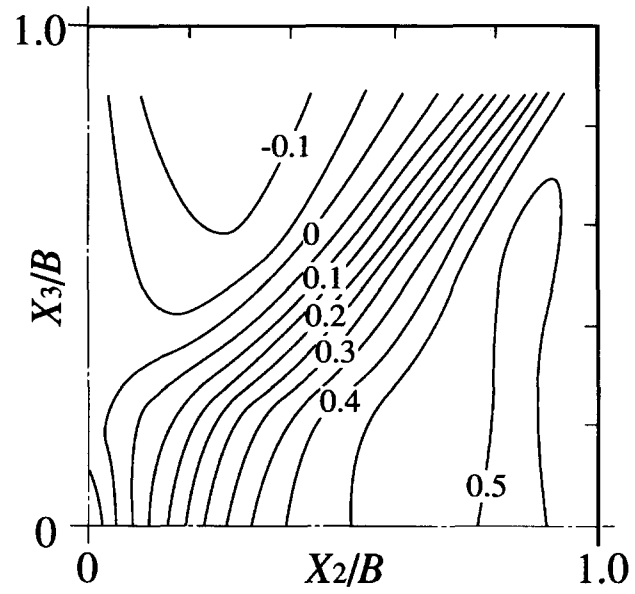

Figure 14 Contour map of R_{12} (cross-correlation between u_1 and u_2)

symmetric with respect to the diagonal of the duct cross section, satisfying the symmetric condition of the flow and temperature fields. This means that there are no essential differences between the distributions of R_{2t} and R_{3t} obtained in the present experiment. Therefore, hereafter we give our attention to momentum and heat transport by u_2 only.

Figure 14 is the contour map of $R_{12} = \overline{u_1 u_2} / \sqrt{\overline{u_1^2}} \cdot \sqrt{\overline{u_2^2}}$, correlation coefficient between the fluctuating velocities u_1 and u_2, which corresponds to R_{2t}, shown in Figure 12. From a detailed comparison of R_{12} and R_{2t}, it is found that the distribution of R_{2t} is qualitatively similar to that of R_{12} but the absolute values of R_{2t} are smaller than those of R_{12}. This quantitative difference between R_{12} and R_{2t} is also observed in turbulent heat transfer in a circular pipe (Hishida et al. 1986).

Turbulent heat fluxes

Figure 15 shows the distribution of $-\overline{u_1 t}$, the turbulent heat flux in the X_1-direction, which is made dimensionless by U_C and $(T_W - T_C)$. Similar to the distributions of $\sqrt{\overline{u_1^2}}$ and $\sqrt{\overline{t^2}}$ shown in Figures 8 and 9, the contours of $-\overline{u_1 t}$ are greatly distorted toward the duct corner. The values of $-\overline{u_1 t}$ reach local minimums on the diagonal of the cross section and increase as the duct walls are approached. It has been found that, dissimilar to R_{1t} distribution shown in Figure 10, the values of $-\overline{u_1 t}$ do not become constant in the near-wall region, and they decrease as the distances from the walls are increased.

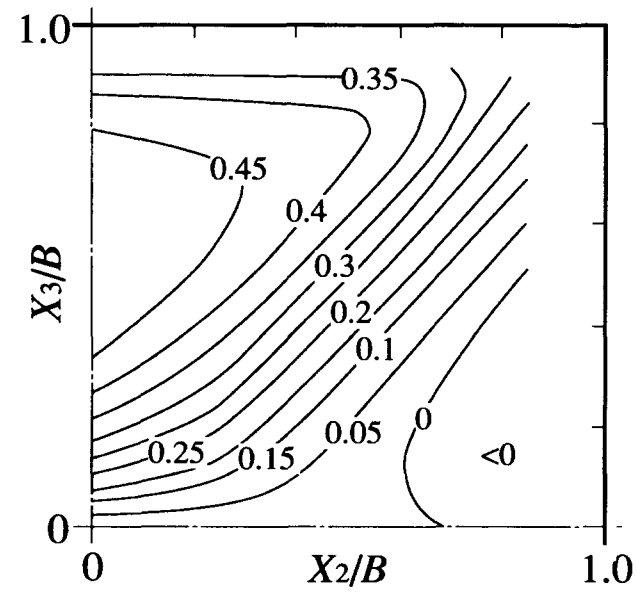

Figure 13 Contour map of R_{3t} (cross-correlation coefficient between u_3 and t)

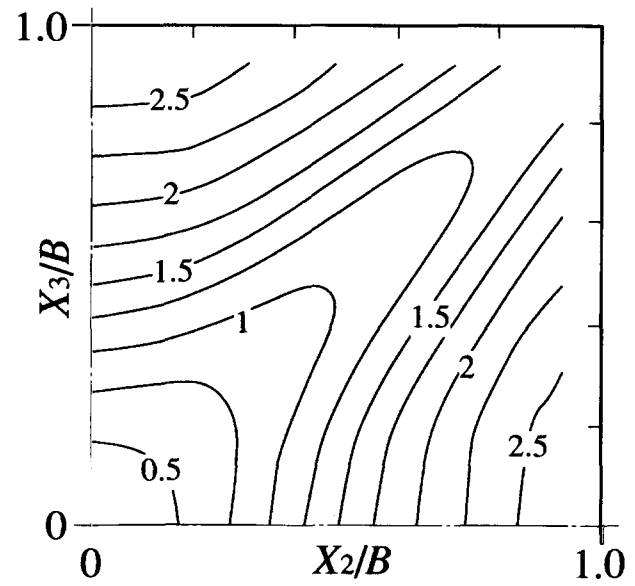

Figure 15 Contour map of turbulent heat flux, $-\overline{u_1 t}/U_C \cdot (T_W - T_C) \times 10^3$

The contour map of the turbulent heat flux in the X_2-direction $-\overline{u_2t}$ is shown in Figure 16. The values of $-\overline{u_2t}$ increase as the side wall $X_2/B = 1$ is approached, and the global characteristics of $-\overline{u_2t}$ distribution are quite similar to those of R_{2t} shown in Figure 12. However, if we compare Figure 16 with Figure 12 in detail, it is found that near the side wall, the characteristics of the $\overline{u_2t}$ distributions are somewhat different from those of R_{2t}. As observed in Figure 12 and described above, R_{2t} near the side-wall is almost constant in the X_3-direction over a relatively wide range of X_3/B, but $-\overline{u_2t}$ in the corresponding region decreases gradually toward the duct corner and is not constant in the X_3-direction. This means that turbulent heat transport from the side wall by u_2 is suppressed as the top wall is approached. It should be also noted that the values of $-\overline{u_2t}$ extrapolated in the X_2-direction to the side wall do not agree with those of the local wall heat flux q_w, because thermal energy is transported in the X_2-direction by not only the fluctuating velocity u_2 but also the mean secondary flow velocity U_2.

Near the intersection of the X_3-axis and the top wall, as expected from the R_{2t} distribution in Figure 12, there exists a negative-value region enclosed by the contour of $-\overline{u_2t} = 0$. As we describe in detail later, this negative-value region in $-\overline{u_2t}$ is peculiar to the turbulent temperature field in forced-convection heat transfer in a square duct accompanied by secondary flow of the second kind.

Figure 17 shows the distribution of the turbulent shear stress $\overline{u_1u_2}$, which corresponds to $-\overline{u_2t}$ shown above. We confirmed that the present distribution of $\overline{u_1u_2}$ obtained in the heated flow condition agreed well with that measured in the isothermal (unheated) flow condition qualitatively and quantitatively. There exists a negative-value region enclosed by the contour of $\overline{u_1u_2} = 0$ near the intersection of the X_3-axis and the top wall, and it follows that the global distribution of $\overline{u_1u_2}$ is qualitatively similar to that of $-\overline{u_2t}$. This suggests that there exists a strong similarity between the turbulent transport processes of momentum and heat even in such a complex turbulent flow accompanied by the secondary flow. If we compare $\overline{u_1u_2}$ with $-\overline{u_2t}$ in detail, however, some differences, such as the size of negative-value region near the X_3-axis, can be also found.

Next, we examine the origin of the negative-value region observed near the X_3-axis of $-\overline{u_2t}$ (Figure 16) and $\overline{u_1u_2}$ (Figure 17) contour maps. In general, the negative-value regions observed in the turbulent shear stress $\overline{u_1u_2}$ in a square duct can be related to the distortion of the primary flow velocity (U_1) distribution by assuming the following equation.

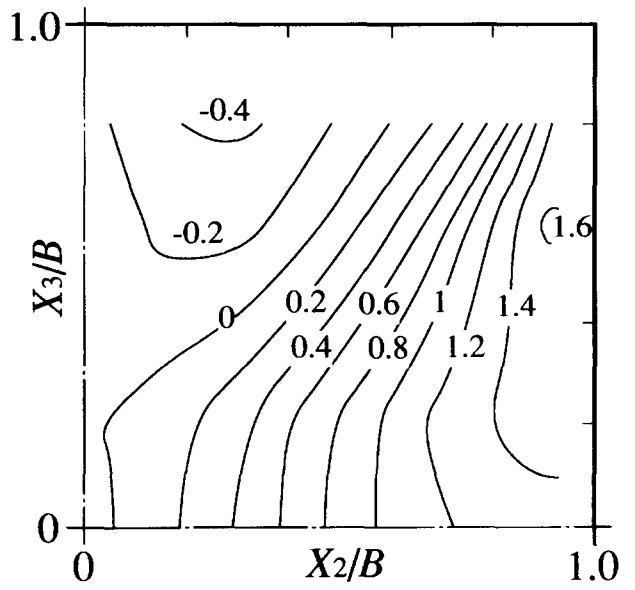

Figure 17 Contour map of turbulent shear stress, $\overline{u_1u_2}/U_C^2 \times 10^3$

$$\overline{u_1u_2} = -\varepsilon_{M2}\frac{\partial U_1}{\partial X_2} \tag{4}$$

where ε_{M2} denotes the eddy kinematic viscosity. Figure 18 shows the mean velocity gradient in the X_2-direction $-\partial U_1/\partial X_2$, which appears on the right-hand side of Equation 4 and has been obtained based on the present experimental results shown in Figure 4. As is well known and also observed in Figure 4, in turbulent flow through a straight square duct, the U_1 contours

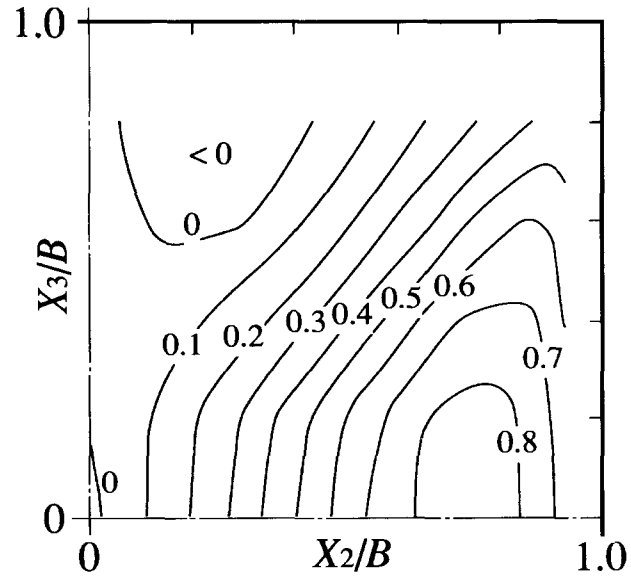

Figure 16 Contour map of turbulent heat flux, $-\overline{u_2t}/U_C \cdot (T_W - T_C) \times 10^3$

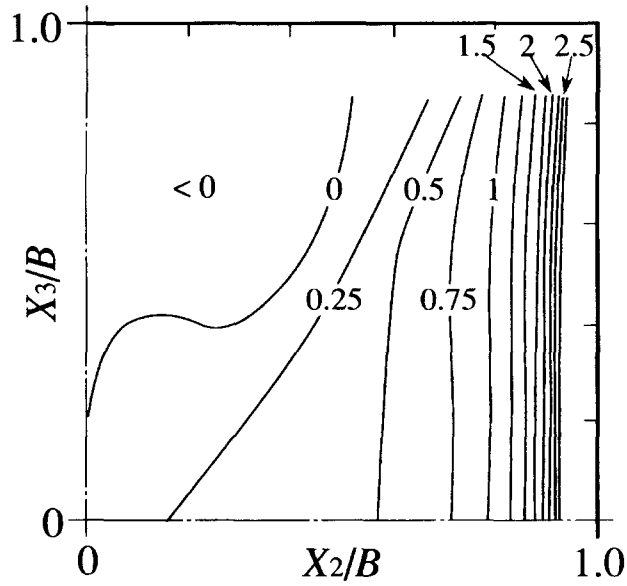

Figure 18 Mean velocity gradient, $-\partial U_1/\partial X_2 \cdot D/U_C$

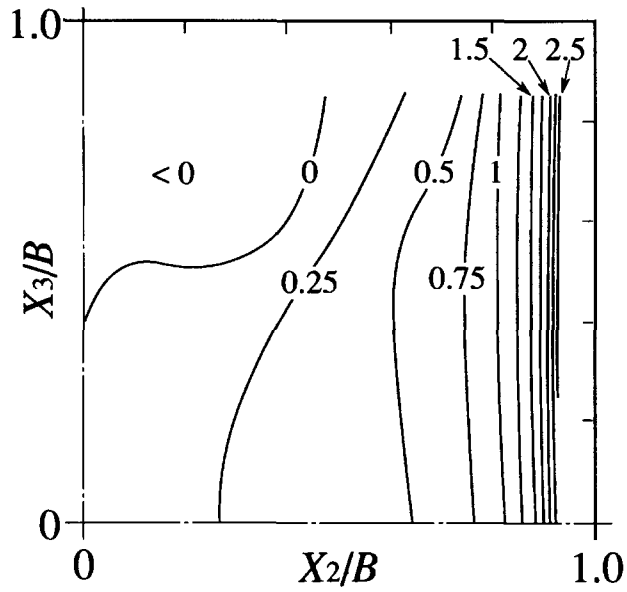

Figure 19 Mean temperature gradient, $\partial T/\partial X_2 \cdot D/(T_W - T_C)$

near the wall bisectors are curved inward owing to the momentum transport by secondary flow of the second kind, which proceeds toward the duct center along the wall bisectors. These inward curves of U_1 contours toward the center correspond to the negative-value region observed near the X_3-axis of $-\partial U_1/\partial X_2$ distribution in Figure 18. From a comparison of Figure 18 and $\overline{u_1 u_2}$ in Figure 17, it is found that the negative-value region in $-\partial U_1/\partial X_2$ corresponds well to that in $\overline{u_1 u_2}$. Therefore, it seems reasonable to assume Equation 4 in order to explain qualitatively the origin of the negative-value region in $\overline{u_1 u_2}$.

In the same way as described above, we assume the following equation to explain the origin of the negative-value region in $-\overline{u_2 t}$.

$$\overline{u_2 t} = -\varepsilon_{H2} \frac{\partial T}{\partial X_2} \tag{5}$$

where ε_{H2} is the eddy thermal diffusivity. Figure 19 is the contour map of $\partial T/\partial X_2$. The distribution of $\partial T/\partial X_2$ is quite similar to that of $\partial U_1/\partial X_2$ shown in Figure 18, and the negative-value region can be observed near the X_3-axis. However, the size of the negative-value region in $\partial T/\partial X_2$ is smaller than that in $\partial U_1/\partial X_2$. This difference corresponds to the fact that the distortion of T contours observed in Figure 5 is weaker than that of U_1 contours in Figure 4, and suggests again that the secondary flow exerts less influence on the mean temperature field than on the mean velocity field. As observed in Figures 16 and 17, the negative-value region in the $-\overline{u_2 t}$ distribution is also smaller in size than that of $\overline{u_1 u_2}$, and the location of the negative-value region in $\partial T/\partial X_2$ agrees well with that observed in $-\overline{u_2 t}$ contours. From these results, it follows that the negative-value regions observed in $\overline{u_1 u_2}$ and $-\overline{u_2 t}$ distributions clearly reflect the effects of momentum and heat transport by secondary flow of the second kind.

Eddy-diffusivities

On the basis of the measured results shown above, we have calculated the values of the eddy kinematic viscosity ε_{M2} and eddy thermal diffusivity ε_{H2} defined in Equations 4 and 5,

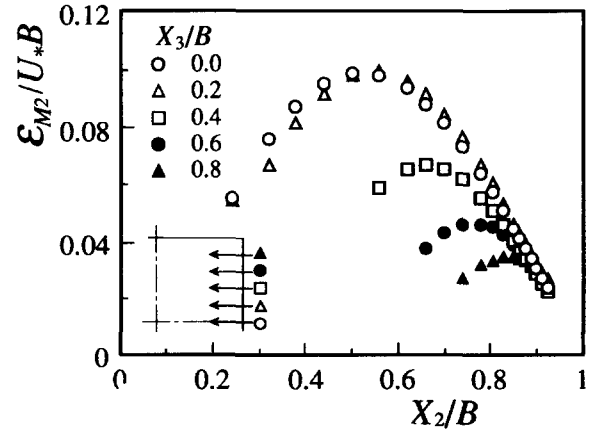

Figure 20 Eddy kinematic viscosity, ε_{M2}/U^*B

respectively. As observed in Figures 18 and 19, however, the values of $\partial U_1/\partial X_2$ and $\partial T/\partial X_2$ are very small in the region far from the side wall, and, consequently, the errors which arise in calculating ε_{M2} and ε_{H2} may become considerably large there. Thus, in this paper, we show the results obtained in the 1/8 cross section enclosed by the side wall, diagonal, and the X_2-axis.

At first, we show the distributions of ε_{M2} in Figure 20, which have been obtained on the lines normal to the side wall; i.e., parallel to the X_2-axis. On the X_2-axis ($X_3/B = 0$), ε_{M2} increases as the distance to the side wall is increased, then attains a maximum value at the midpoint between the side wall and the duct center and decreases toward the duct center. This distribution is quite similar to that of the turbulent flow through a circular pipe (Schlichting 1979). As the top wall is approached, the values of ε_{M2} become smaller, and the maximum values appear in locations nearer the side-wall.

Figure 21 shows distributions of the eddy thermal diffusivity ε_{H2}. The distributions are qualitatively similar to those of ε_{M2} described above. However, from a quantitative viewpoint, it is found that the values of ε_{H2} are generally smaller than those of ε_{M2}. Considering that ε_{M2} ((ε_{H2}) and ε_{M3} (ε_{H3}) are symmetric with respect to the diagonal of the duct cross section, it follows that the eddy-viscosities and eddy thermal diffusivities in the square duct have a quite anisotropic feature.

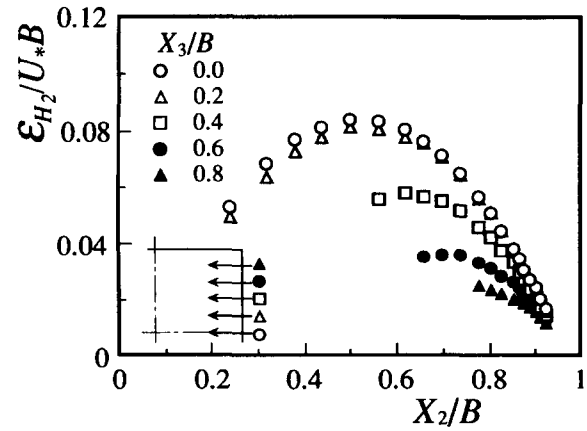

Figure 21 Eddy thermal diffusivity, ε_{H2}/U^*B

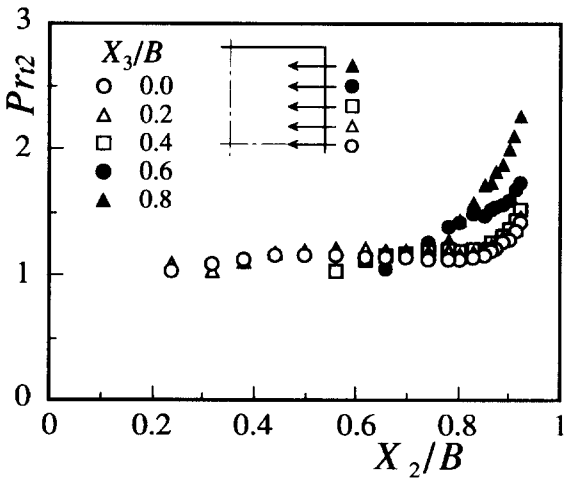

Figure 22 Turbulent Prandtl number

Turbulent Prandtl number

Based on the results of ε_{M2} and ε_{H2} shown above, we have obtained distributions of the turbulent Prandtl number Pr_{t2}, which is defined by the following equation.

$$\mathrm{Pr}_{t2} = \frac{\varepsilon_{M2}}{\varepsilon_{H2}} \tag{6}$$

Figure 22 shows distributions of Pr_{t2} obtained on lines normal to the side wall. On the X_2-axis, the values of Pr_{t2} become almost constant over a wide range of X_2/B and then increase as the side wall ($X_2/B = 1.0$) is approached. Such characteristics of Pr_{t2} distribution on the X_2-axis of the present test duct are quite similar to those obtained for turbulent heat transfer in a circular pipe (Hishida et al. 1986). This suggests that, on the axes of symmetry of the square duct, the influences of the adjacent wall and the secondary flow on the turbulent Prandtl number distributions are not very large. As the duct corner is approached, the values of Pr_{t2} becomes larger, and the region in which Pr_{t2} is approximately constant becomes narrower. These results mean that the assumption of constant turbulent Prandtl number often used in the numerical simulation of the turbulent heat transfer in a square duct (Launder and Ying 1973, Myong 1991) is not valid near the corner of the duct.

Next, we discuss the definition of the turbulent Prandtl number in the complex turbulent flow through a square duct, based on the production mechanisms of the turbulent heat flux $\overline{u_2 t}$ and turbulent shear stress $\overline{u_1 u_2}$. In general, the production term in the transport equation of the turbulent heat flux $\overline{u_i t}$ (denoted as P_{it}, $i = 1$, 2, or 3) can be described as follows (Launder 1988).

$$P_{it} = -\overline{u_i u_j}\frac{\partial T}{\partial X_j} - \overline{u_j t}\frac{\partial U_i}{\partial X_j} \tag{7}$$

For the turbulent heat flux $\overline{u_2 t}$, the production term P_{2t} can be written as follows, assuming that turbulent flow and temperature fields are fully developed in the streamwise direction; i.e., $\partial/\partial X_1 = 0$.

$$P_{2t} = -\overline{u_2^2}\frac{\partial T}{\partial X_2} - \overline{u_2 u_3}\frac{\partial T}{\partial X_3} - \overline{u_2 t}\frac{\partial U_2}{\partial X_2} - \overline{u_3 t}\frac{\partial U_2}{\partial X_3} \tag{8}$$

Similar to P_{2t}, the production term of turbulent shear stress $\overline{u_1 u_2}$ (denoted as P_{12}) can be expressed by the following equation.

$$P_{12} = -\overline{u_2^2}\frac{\partial U_1}{\partial X_2} - \overline{u_2 u_3}\frac{\partial U_1}{\partial X_3} - \overline{u_1 u_2}\frac{\partial U_2}{\partial X_2} - \overline{u_1 u_3}\frac{\partial U_2}{\partial X_3} \tag{9}$$

On the X_2-axis in which the Pr_{t2} distribution in the present square duct agrees well with that in the circular pipe, the second and fourth terms on the right-hand side of Equations 8 and 9 become zero because of the condition of symmetry. Because the values of $\partial T/\partial X_2$ and $\partial U_1/\partial X_2$ are far larger than those of $\partial U_2/\partial X_2$, the productions of $\overline{u_2 t}$ and $\overline{u_1 u_2}$ on the X_2-axis of the square duct are mainly brought about by the contributions of the first term of Equations 8 and 9. This mechanism of $\overline{u_2 t}$ and $\overline{u_1 u_2}$ productions on the X_2-axis is similar to that of the circular pipe, and in the definitions of eddy-diffusivities ε_{M2} and ε_{H2} in Equations 4 and 5, only the contributions of $\partial T/\partial X_2$ and $\partial U_1/\partial X_2$ are considered. It is thought, therefore, that the distributions of the eddy-diffusivities ε_{M2} and ε_{H2}, and those of the turbulent Prandtl numbers Pr_{t2} on the X_2-axis of the present duct become quite similar to those of the circular pipe.

On the other hand, as the top wall is approached, the contributions of the other terms in Equations 8 and 9 become more significant. In particular, near the duct corner, it is estimated that the contributions of the second term involving $\partial T/\partial X_3$ or $\partial U_1/\partial X_3$ become as large as those of the first term. However, as recognized from Equations 4 and 5, the contributions of these second terms are not involved in the present definitions of the eddy-diffusivities ε_{M2} and ε_{H2}. Therefore, it follows that the definitions of the eddy-diffusivities given by Equations 4 and 5 may become invalid near the corner of the square duct, although they are effective to explain qualitatively the origin of the negative-value regions in $\overline{u_2 t}$ and $\overline{u_1 u_2}$ contours. In the numerical simulation of convective heat transfer in complex turbulent flows, we should not use the traditional eddy-diffusivity concept too easily, and the concept such as the WET hypothesis (Launder 1988) that does not use eddy-diffusivities seems to be more reasonable than the usual turbulent Prandtl number to express the turbulent heat fluxes. For a detailed discussion on the production process of the turbulent heat fluxes and improvement of the eddy-diffusivity concept, however, it is important to make clear quantitatively the contributions of each term of Equations 8 and 9. In particular, distributions of the turbulent shear stress $\overline{u_2 u_3}$, which is also important for the production of the secondary flow of the second kind (Demuren and Rodi 1984, Kajishima et al. 1991) and very difficult to measure with high accuracy, should be made clear by detailed experiments or numerical simulations.

Conclusions

Detailed measurements have been conducted on the forced-convection heat transfer for turbulent flow in a straight, square duct, and distributions of the mean temperature, fluctuating temperature intensity, correlation coefficients, and turbulent heat fluxes have been made clear. The eddy-diffusivities and turbulent Prandtl number have also been obtained based on the experimental data. The results obtained here can be summarized as follows.

(1) The distributions of the mean temperature in the present test duct are similar to those of the mean primary flow velocity and are curved inward toward the duct center near the wall

bisectors of the duct cross section. The distortions of the mean temperature contours are, however, weaker than those of the primary flow velocity.

(2) The cross-correlation coefficient between u_1 and t; i.e., R_{1t}, is almost constant near the duct walls, and it decreases toward the duct center. The region in which R_{1t} is nearly constant becomes narrower near the duct corner. R_{2t} is also almost constant in the X_3-direction near the side-wall of the duct. However, the region of constant R_{2t} value becomes narrower as the distance from the side-wall increases, and the values of R_{2t} decrease as the duct corner is approached.

(3) The contours of the turbulent heat flux $-\overline{u_1 t}$ are sharply distorted toward the duct corner, behavior similar to that observed for the fluctuating temperature intensity. Dissimilar to the R_{1t} distributions described above, the values of $-\overline{u_1 t}$ do not become constant in the near-wall region, and they decrease as distances from the duct walls are increased.

(4) The distributions of the turbulent heat flux $-\overline{u_2 t}$ are qualitatively similar to those of the turbulent shear stress $\overline{u_1 u_2}$, and negative-value regions appear near the X_3-axis of the $-\overline{u_2 t}$ and $\overline{u_1 u_2}$ contour maps. Those negative-value regions in $-\overline{u_2 t}$ and $\overline{u_1 u_2}$ correspond well to those in $\partial T/\partial X_2$ and $\partial U_1/\partial X_2$ distributions.

(5) The distributions of the eddy thermal diffusivity ε_{H2} on the X_2-axis of the test duct are similar to those of the eddy kinematic viscosity ε_{M2} in the circular pipe, which attains a maximum value at the midpoint between the side wall and the duct center. As the top wall is approached, however, the values of ε_{H2} become smaller, and the maximum values appear in locations nearer the side wall. The distributions of the eddy kinematic viscosity ε_{M2} in the full quadrant are qualitatively similar to those of ε_{H2}, but the values of ε_{M2} are larger than those of ε_{H2}.

(6) The turbulent Prandtl number Pr_{t2} shows an almost constant value on the X_2-axis over a wide range of X_2/B. As the adjacent top wall is approached, the values of Pr_{t2} increase, and the region in which Pr_{t2} is approximately constant becomes narrower.

Acknowledgments

The authors express their thanks to N. Kasagi at University of Tokyo for his valuable advice. They also thank N. Shiraki and K. Tachibana, research engineers of Nagoya University, for their cooperation in building the experimental apparatus. A part of this research was supported by the Japanese Ministry of Education through a Grant-in-Aid for Scientific Research (Grant No. 05750188).

References

Alexopoulos, C. C. 1964. Temperature and velocity distributions and heat transfer for turbulent air flow in a square duct. M.A. Thesis, Dept. Mech. Eng., University of Toronto, Toronto, Canada

Brundrett, E. and Burroughs, P. R. 1967. The temperature inner-law and heat transfer for turbulent flow in a vertical square duct. *Int. J. Heat Mass Transfer*, **10** 1133–1142

Demuren, A. O. and Rodi, W. 1984. Calculation of turbulence-driven secondary motion in noncircular ducts. *J. Fluid Mech.*, **140,** 189–222

Emery, A. F., Neighbors, P. K. and Gessner, F. B. 1980. The numerical prediction of developing turbulent flow and heat transfer in a square duct. *J. Heat Transfer*, **102,** 51–57

Fujita, H., Hirota, M., Yokosawa, H., Hasegawa, M. and Gotoh, I. 1990. Fully developed turbulent flows through rectangular ducts with one roughened wall. *JSME Int. J.*, Ser. II, **33,** 692–701

Fujita, H., Yokosawa, H. and Hirota, M. 1989. Secondary flow of the second kind in rectangular ducts with one rough wall. *Exp. Therm. Fluid Sci.*, **2,** 72–80

Fujita, H., Yokosawa, H., Hirota, M. and Nagata, C. 1988. Fully developed turbulent flow and heat transfer in a square duct with two roughened facing walls. *Chem. Eng. Comm.*, **74,** 95–110

Gavrilakis, S. 1992. Numerical simulation of low-Reynolds-number turbulent flow through a straight square duct. *J. Fluid Mech.*, **244,** 101–129

Gessner, F. B. 1981. Corner flow (secondary flow of the second kind). *Proc. 1980-AFOSR-HTTM-Stanford Conference on Complex Turbulent Flows*, 182–212

Gessner, F. B. and Emery, A. F. 1976. A Reynolds stress model for turbulent corner flows—Part I: Development of the model. *J. Fluids Eng.*, **98,** 261–268

Gessner, F. B. and Po, J. K. 1976. A Reynolds stress model for turbulent corner flows—Part II: Comparison between theory and experiment. *J. Fluids Eng.*, **98,** 269–277

Gessner, F. B., Po, J. K. and Emery, A. F. 1979. Measurements of developing turbulent flow in a square duct. In *Turbulent Shear Flows 1*, F. Durst et al. (eds.), Springer, New York, 119–136

Hayase, T. and Suematsu, Y. 1991. Direct numerical simulation of turbulent flow in a square pipe. In *Flucome '91*, W. C. Yang and R. L. Woods (eds.), ASME, New York, 99–106

Hirota, M., Fujita, H. and Yokosawa, H. 1988. Influences of velocity gradient on hot-wire anemometry with an X-wire probe. *J. Phys E: Sci. Instrum.*, **21,** 1077–1084

Hirota, M., Fujita, H. and Yokosawa, H. 1994. Experimental study on convective heat transfer for turbulent flow in a square duct with a ribbed rough wall (characteristics of mean temperature field). *J. Heat Transfer*, **116,** 332–340

Hishida, M. and Nagano, Y. 1978. Simultaneous measurements of velocity and temperature in nonisothermal flows. *J. Heat Transfer*, **100,** 340–345

Hishida, M. and Nagano, Y. 1979. Structure of turbulent velocity and temperature fluctuations in fully developed pipe flow. *J. Heat Transfer*, **101,** 15–22

Hisida, M., Nagano, Y. and Tagawa, M. 1986. Transport processes of heat and momentum in the wall region of turbulent pipe flow. *Proc. 8th International Heat Transfer Conference*, **3,** 925–930

Huser, A. and Biringen, S. 1993. Direct numerical simulation of turbulent flow in a square duct. *J. Fluid Mech.*, **257,** 65–95

Huser, A., Biringen, S. and Hatay, F. F. 1994. Direct simulation of turbulent flow in a square duct: Reynolds-stress budgets. *Phys. Fluids*, **6,** 3144–3152

Johnston, J. P. 1976. Internal flows. In *Turbulence* P. Bradshaw (ed.), Springer, New York, 109–169

Kajishima, T., Miyake, Y. and Nishimoto, T. 1991. Large-eddy simulation of turbulent flow in a square duct. *Trans. JSME (B)*, **57,** 2530–2537 (in Japanese)

Launder, B. E. 1988. On the computation of convective heat transfer in complex turbulent flows. *J. Heat Transfer*, **110,** 1112–1228

Launder, B. E. and Ying, W. M. 1973. Prediction of flow and heat transfer in ducts of square cross-section. *Proc. Inst. Mech. Eng.*, **187,** 455–461

Madabhushi, R. and Vanka, S. P. 1991. Large-eddy simulation of turbulence-driven secondary flow in a square duct. *Phys. Fluids A*, **3,** 2734–2745

Melling, A. and Whitelaw, J. H. 1976. Turbulent flow in a rectangular duct. *J. Fluid Mech.*, **78,** 289–315

Myong, H. K. 1991. Numerical investigation of fully developed turbulent fluid flow and heat transfer in a square duct. *Int. J. Heat Fluid Flow*, **12,** 344–352

Nakayama, A., Chow, W. L. and Sharma, D. 1983. Calculation of fully developed turbulent flows in ducts of arbitrary cross-section. *J. Fluid Mech.*, **128,** 199–217

Nakayama, A. and Koyama, H. 1986. Numerical prediction of turbulent flow and heat transfer within ducts of cross-shaped cross section. *J. Heat Transfer*, **108,** 841–847

Nishijima, S. 1989. A numerical study of turbulent square-duct flow using an anisotropic k-ε model. *Trans. JSME (B)*, **55,** 991–998 (in Japanese)

Patel, V. C. 1965. Calibration of the Preston tube and limitations on its use in pressure gradients. *J. Fluid Mech.*, **23,** 185–208

Schlichting, H. 1979. *Boundary Layer Theory*, 7th ed. McGraw-Hill, New York, 609

Speziale, C. G. 1987. On nonlinear K-l and K-ε models of turbulence. *J. Fluid Mech.*, **178,** 459–475

Sugiyama, H., Akiyama, M. and Matsumoto, M. 1995. Numerical analysis of turbulent structure and heat transfer in a square duct with one rough wall. *Thermal Eng.*, **1,** 409–416

Sugiyama, H., Akiyama, M., Matsumoto, M., Hirata, M. and Ninomiya, N. 1993. Numerical analysis of fully developed turbulent flow in a square duct with two facing roughened walls. *Comp. Fluid Dynamics*, **2,** 319–338

Yokosawa, H., Fujita, H., Hirota, M. and Iwata, S. 1989. Measurement of turbulent flow in a square duct with roughened walls on two opposite sides. *Int. J. Heat Fluid Flow*, **10,** 125–130